JOURNAL OF AIRCRAFT
Vol. 43, No. 4, July–August 2006

Establishment of Gun Blast Wave Model and Structural Analysis for Blast Load

Dae-Kwan Kim* and Jae-Hung Han†
Korea Advanced Institute of Science and Technology, Daejeon 305-701, Republic of Korea

DOI: 10.2514/1.18250

The muzzle of a gun mounted on an airplane emits repetitive gun blast waves during the firing. These blast waves expand in open space and they are reflected on the airplane surface adjacent to the gun. The vibration resulting from the reflected waves can cause adverse effects to the airplane. Therefore, it is very important to establish an accurate blast wave model for the prediction of the vibration level. In the present study, the blast wave model is established using a scaling approach and CFD calculation, and this model is verified with experimental data. The established blast wave model is applied to two kinds of structural models. First, to investigate the effect of the muzzle distance from the surface, the responses of a graphite epoxy composite panel exposed to the blast wave are analyzed for various muzzle distances. Second, the transient response analyses of a left wing model are carried out for several repeated fires. From the results, it can be shown that the assumption of uniform blast wave is not applicable in the near muzzle distance, and the vibration resulting from the repetitive blast waves can cause high frequency damage to the structure and equipments mounted in the aircraft.

Nomenclature

a_m	=	muzzle sound speed
a_∞	=	ambient sound speed
C_P	=	reflected pressure coefficient
D	=	bore diameter of gun
h	=	muzzle distance
M	=	Mach number
P	=	incident overpressure
P_I	=	incident pressure (incident blast wave)
$\bar{P}_I$	=	peak incident overpressure
$\tilde{P}_I$	=	nondimensional incident overpressure
P_R	=	reflected pressure (reflected blast wave)
$\bar{P}_R$	=	peak reflected overpressure
P_m	=	muzzle pressure
P_∞	=	ambient pressure
t_a	=	blast arrival time
V_p	=	exit velocity of projectile
$\boldsymbol{v}$	=	vector directed from boreline to reflecting point
α_i	=	incident angle
γ	=	specific heat ratio
δ_i	=	deflection angle
θ_i	=	reflection angle
σ	=	normalized rms deviation
τ	=	positive phase duration

I. Introduction

IN recent years, helicopters and aircrafts have been equipped with integrated weapon systems such as Heavy Machine Gun Pod to improve their fighting power. While firing, the gun muzzle emits repetitive blast waves as shown in Fig. 1, which are shock waves expanding from the muzzle. These waves travel in open space and their strength is determined by the weapon characteristics and launch conditions. They are then reflected on the surface adjacent to the gun. The reflection of these blast waves can be a regular reflection or a Mach reflection, depending on the strength and the incident angle to the reflecting surface of the traveling wave. The vibration resulting from the reflected shock waves is 2 orders of magnitude, about normal flight vibration levels. This vibration can cause adverse effects such as intermittent electrical contact, catastrophic electrical failures, hydraulic malfunctions, and structure fatigue failures to the structure or equipment mounted in the aircraft. Especially, these effects are quite serious when the firing gun muzzle is close to the structural skin and the equipment which should physically and functionally withstand the vibration levels. Therefore, it is very important to establish an accurate blast wave model and to analyze the response of the structure subjected to the blast wave for the prediction of the vibration levels on the skin and equipment.

While there have been many studies on modeling and analysis of the flow field about a muzzle, the published research articles on structural vibration resulting from the blast wave of a gun mounted on military aircraft are not sufficient because of military confidentiality and experimental difficulty. Erdos and Del Guidice [1] represented the unsteady flow field between the Mach disk and the blast wave consequent to the firing of a M16 rifle, developing a finite difference solution. Schmidt and Shear [2] measured the flow

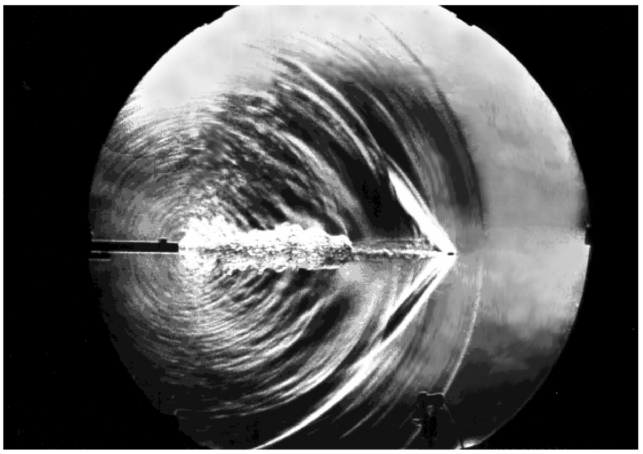

Fig. 1 Instantaneous image of bullet and muzzle blast from 22-caliber rifle [15].

Presented as Paper 2261 at the 46th AIAA/ASME/ASCE/AHS/ASC Structures, Structural Dynamics & Materials Conference, Austin, Texas, 18–21 April 2005; received 16 June 2005; accepted for publication 24 December 2005.

*Graduate Research Assistant, Department of Aerospace Engineering; dkk@asdl.kaist.ac.kr.

†Assistant Professor, Department of Aerospace Engineering; jaehunghan@kaist.ac.kr. Member AIAA.

field around the muzzle of a M16 rifle by using a time-resolved, spark shadowgraph system, and they illustrated the progress of the flow structure in detail. Moretti [3] introduced a new computational technique to solve the Navier–Stokes equations for the flow field induced by the firing of a gun, and compared the results of the numerical analysis with experimental data. To improve the prediction of a blast impulse using a scaling approach, Fansler [4] investigated the characteristic exhaust decay time for the energy efflux at the jet exit of guns and shock tubes. Heaps et al. [5] extended a free field muzzle blast scaling technique to consider the blast wave reflection from surfaces by using an analytic solution of the regular reflection and curve fit functions extracted from experimental data. They also developed a computer code that generates contour maps of a reflected blast wave model described by a function of peak reflected overpressure, blast wave time of arrival, and blast wave positive phase duration. Gupta et al. [6] used closed-form solutions of a rectangular plate to analyze the responses of the plate subjected to the explosive uniform blast load generated by the use of Friedlander decay function for linear and nonlinear dynamic cases. Louca et al. [7] investigated the effects of boundary conditions on the dynamic responses of panels subjected to uniform blast loading, which assumed as a symmetrical, positive triangular pulse. Na and Librescu [8] performed studies of the control of dynamic responses of nonuniform thin-walled beam cantilevers to explosive blast, sonic-boom, rectangular, and step pressure pulses, using structural tailoring and adaptive materials technique. Librescu et al. [9] investigated the linear and nonlinear dynamic responses of sandwich panels to sea water and air blast loadings which were assumed to be uniform over the entire panels. Librescu et al. [10] simulated the active aeroelastic control of 2-D wing-flap systems operating in an incompressible flowfield and exposed to a triangular blast loading. Turkmen [11] analyzed the dynamic responses of cylindrically curved laminated composite shells subjected to normal blast loading. The blast pressure and strain measurements are also performed, and the experimental data were compared with the analysis results. But he assumed the whole panel was just exposed to a uniform blast load described by the Friedlander decay function.

In the present study, a blast wave model is established using the scaling approach [5]. To consider the regular and Mach reflections, the analytic solutions of the regular reflection are obtained by using the oblique shock theory, and Mach reflection is numerically calculated by the use of a commercial CFD software FLUENT. The established blast wave model GUNBLAST is verified with experimental data and applied to two kinds of structural models. First, to investigate the effect of the muzzle distance from a surface to the muzzle, the responses of a graphite epoxy composite panel exposed to the blast wave of a 12.7 mm gun are analyzed by using MSC/NASTRAN for various muzzle distances. Second, the transient response analyses of a left wing model with an external fuel tank and a 12.7 mm outboard gun are carried out for 1 and 50 rounds with 17 Hz firing rate.

II. Gun Blast Wave Modeling

After firing a gun, the blast wave emitted from the muzzle expands in open space as a free field blast wave, and this wave is reflected on structural surfaces. As the reflected blast wave contacts the surface, it subjects the structure to an impulse load. The reflection of the blast wave on the surface can be regular reflection or Mach reflection, which depends on the strength of the free field blast wave and the incident angle. To establish the gun blast wave model, therefore, the reflected blast wave as well as the free field blast wave should be considered. In this study, the free field blast wave is calculated by using the scaling approach [5], and this calculation process will be described briefly in this paper. For the calculation of the reflected blast wave, the analytic solution of the regular reflection is obtained by the use of the oblique shock theory, and Mach reflection is numerically calculated by using FLUENT. Finally, the gun blast wave model, GUNBLAST, is verified with experimental data available in the literature.

A. Free Field Blast Wave

1. Scaling Approach

The free field blast wave can be described by the use of the Friedlander waveform [12]. This waveform is a function of the peak incident overpressure $\bar{P}_I$, the blast arrival time t_a, and the positive phase duration τ as shown in Fig. 2. Using this function, the nondimensionalized incident overpressure $\tilde{P}_I$ at an arbitrary grid point in the open space can be written as follows:

$$\tilde{P}_I = (P_I - P_\infty)/P_\infty = \begin{cases} 0, & t < t_a \\ \bar{P}_I[1 - (t - t_a)/\tau]e^{-(t-t_a)/\tau}, & t \geq t_a \end{cases} \tag{1}$$

Figure 2 shows the variation of the blast wave pressure with respect to time at a grid point in an open space. In general, the pressure rises very abruptly after t_a from the ambient pressure in the unaffected air to the positive peak value $\bar{P}_I$ (a,b). It then decreases rapidly to zero overpressure during τ (b,c), and the negative pressure phase follows the positive phase (c,d). During the expansion of the wave, while the arrival time and the positive phase duration increase, the peak incident overpressure decreases. Because the positive phase duration is very short, the blast wave can be considered as an impulse load, and it is more obvious near the muzzle. The negative phase duration, however, should be considered to analyze a structure exposed to the blast wave, because the absence of the negative pressure part may cause the response to be apparently more damped.

To calculate the free field blast wave in the open space using Eq. (1), the three time invariant parameters, $\bar{P}_I$, t_a, and τ, should be determined for each grid point independently, and these parameters depend on weapon characteristics and launch conditions. Figure 3 shows the geometry of the launch conditions of a gun pointed to an arbitrary direction. The origin of the axis is located at the muzzle of the gun and the x–y plane is parallel to the contour plane. The location of any grid point of interest in the contour plane can be determined by the vector $\boldsymbol{r}$ which is defined by the magnitude and the angle between $\boldsymbol{r}$ and $\boldsymbol{u}$. To obtain the launch conditions, therefore, the values of r and θ must be determined for each grid point as follows:

$$r = (x^2 + y^2 + h^2)^{1/2} \tag{2}$$

$$\theta = \cos^{-1}\frac{\boldsymbol{r}\cdot\boldsymbol{u}}{r} \tag{3}$$

with

$$\boldsymbol{u} = 0\boldsymbol{e}_x + \cos\phi\boldsymbol{e}_y + \sin\phi\boldsymbol{e}_z \tag{4}$$

where h, $\boldsymbol{u}$, and ϕ are the height of the muzzle from the contour map, the unit vector of the boreline in the y–z plane and the angle between $\boldsymbol{u}$ and y axis, respectively.

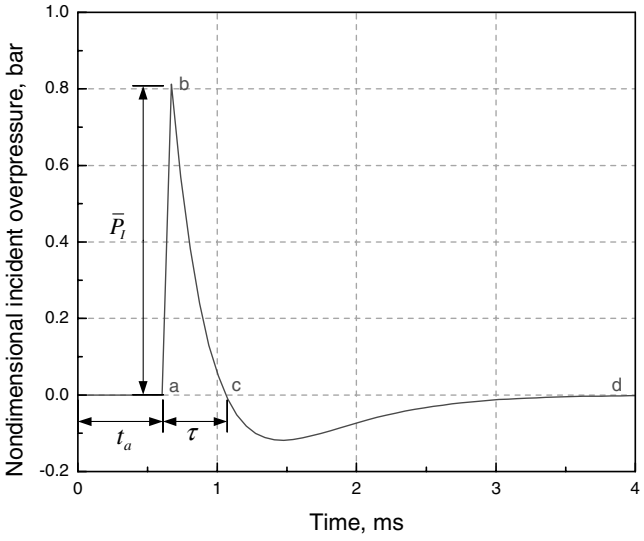

Fig. 2 Variation of blast wave pressure vs time.

Table 1 Parameter values of weapon characteristics and launch conditions

Parameter	Value		Unit
	30 mm gun [5]	12.7 mm gun	
D	30	12.7	mm
h	0.26	0.1–10	m
a_m	920.0	945.209	m/s
a_∞	340.292	340.292	m/s
V_p	780.0	880.0	m/s
ϕ	0.00	0.00	deg
P_m/P_∞	330.0	325.865	
γ	1.24	1.24	
μ	0.78	0.78	

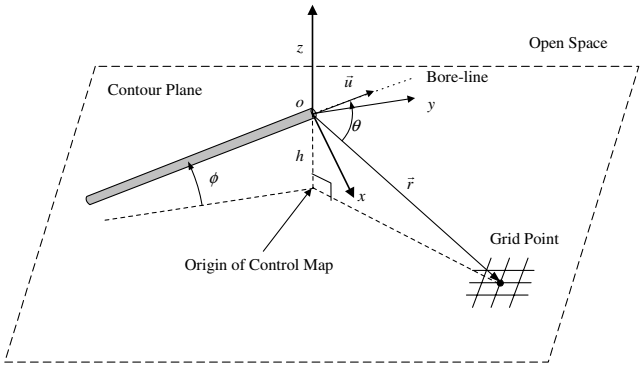

Fig. 3 Geometry of launch conditions.

In the present study, the scaling approach described in [4,5] is used to calculate the three parameters for each grid point in the contour plane of interest, and these parameters can be expressed summarily as follows:

$$\bar{P}_I = 2.4Z \tag{5}$$

$$t_a = \frac{r}{a_\infty} f(Z) - \frac{\ell'}{a_\infty}(0.94\cos\theta + 9.24) \tag{6}$$

$$\tau = (\ell'/a_\infty)[1 + 0.13(r/\ell')] \tag{7}$$

with

$$\ell' = \ell[\mu\cos\theta + (1 - \mu^2\sin^2\theta)^{1/2}] \tag{8}$$

$$Z = (r/\ell')^{-1.1} \tag{9}$$

$$f(Z) = 1 + 10Z - (Z^2/1.2) + (Z^3/2.3) - (Z^4/3.4) + (Z^5/4.5) - (Z^6/5.6) \tag{10}$$

$$\ell = D\left\{\frac{(8.62\times10^{-3})P_m a_m}{(\gamma-1)P_\infty a_\infty}\left[1 + \frac{\gamma(\gamma-1)}{2}\right] \times \left[\frac{2}{\gamma+1}\left(1 + \frac{(\gamma-1)}{2}\frac{V_p}{a_m}\right)\right]^{3(\gamma-1)/\gamma-1}\right\}^{1/2} \quad (V_p \le a_m) \tag{11}$$

and

$$\ell = (9.28\times10^{-2})D\left[\frac{P_m V_p}{(\gamma-1)P_\infty a_\infty}\left(1 + \frac{\gamma(\gamma-1)V_p^2}{2a_m^2}\right)\right] \quad (V_p > a_m) \tag{12}$$

where a_∞ and P_∞ are the ambient sound speed and ambient pressure. The weapon characteristic parameters μ, D, a_m, P_m, V_p, and γ are the momentum index, the diameter of gun, the propellant sound speed at muzzle, the muzzle pressure, the projectile velocity, and the specific heat ratio, respectively.

2. *Characteristics of Free Field Blast Wave*

To investigate the characteristics of the blast wave model obtained by using the Friedlander waveform and the scaling approach, the free field blast wave of a 30 mm chain gun is calculated. The weapon characteristic parameters and the launch conditions used in this blast

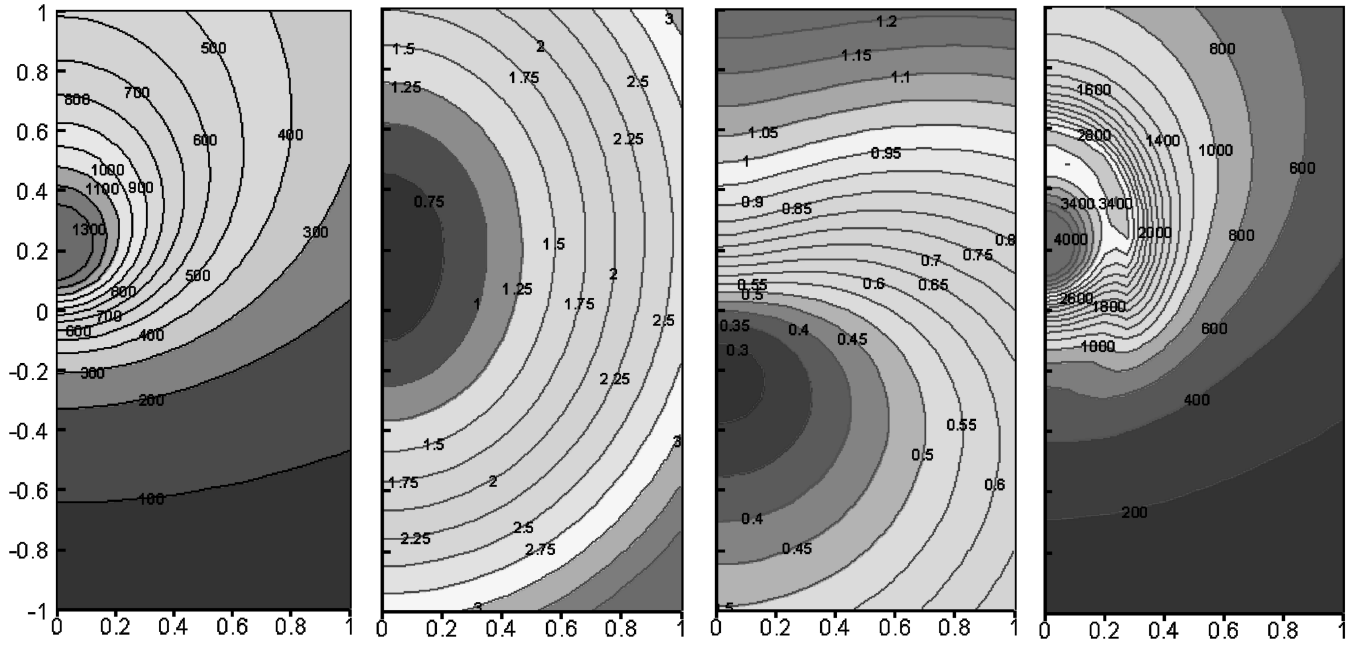

a) $\bar{P}_I$, mbar b) t_a, ms c) τ, ms d) $\bar{P}_R$, mbar

Fig. 4 Parameter contour maps of calculated by GUNBLAST for 30 mm chain gun.

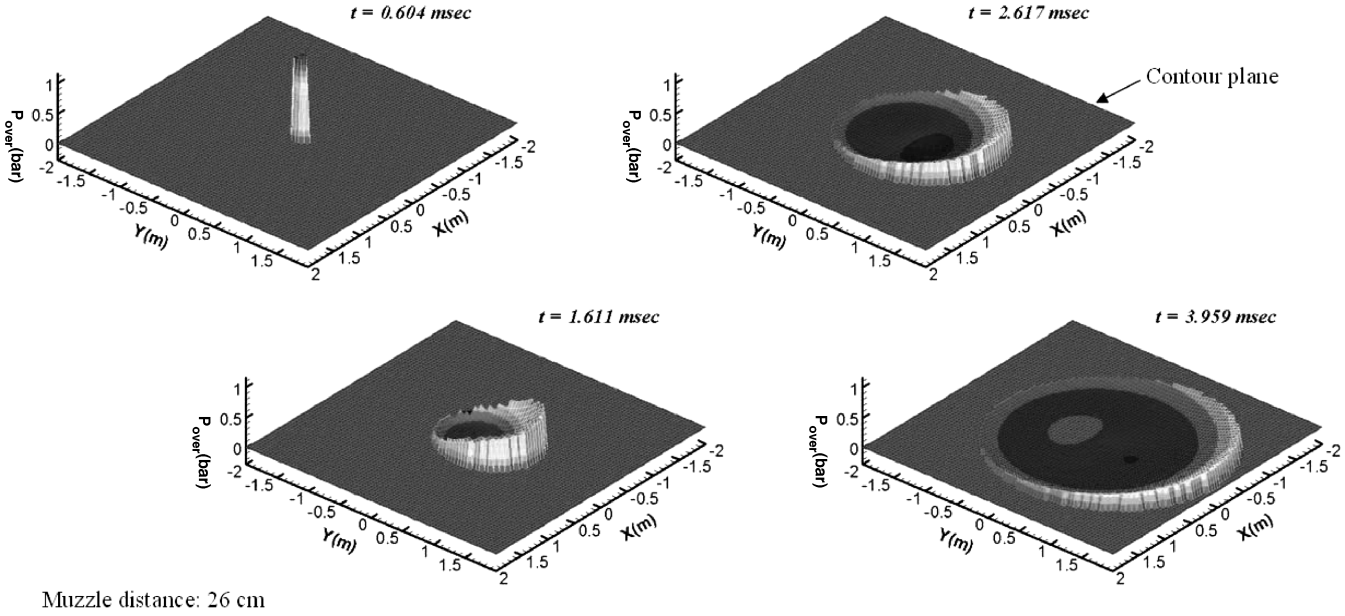

Fig. 5 Simulation results of the free field blast wave for 30 mm chain gun.

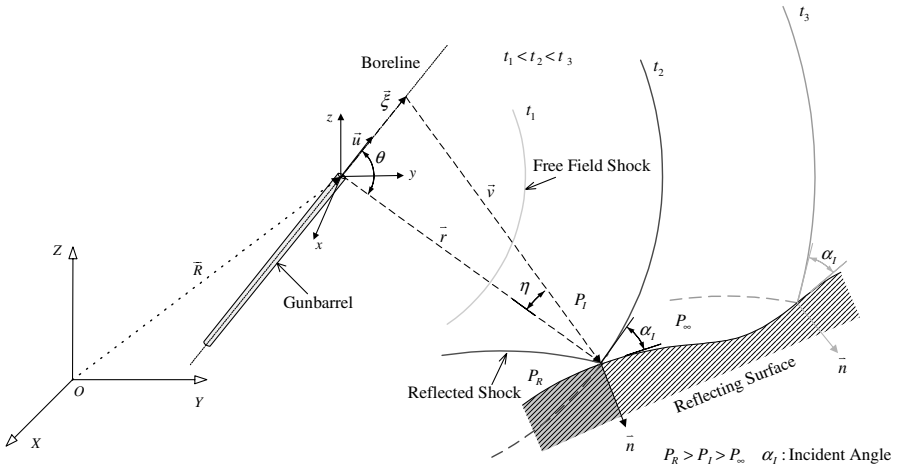

Fig. 6 Schematic diagram of gun blast wave reflection.

wave model are listed in Table. 1. The gun muzzle is parallel to the contour plane, the height of the muzzle is 26 cm, and the open space around the gun is the standard atmospheric condition at sea level.

The contour maps of the three parameters, $\bar{P}_I$, t_a, and τ, calculated by the free field blast wave model are shown in Figs. 4a–4c. The peak incident overpressure decreases circularly with a center located forward from the origin. The blast arrival time decreases almost circularly, and the positive phase duration map shows the rapid increase in the forward direction.

Figure 5 shows the simulation results of the free field blast wave with respect to time. After firing, the blast wave contacts the contour map at 0.604 ms, and it then expands outward direction from the center displaced in the forward direction from the muzzle. It shows that the peak pressure is larger in the forward direction than in backward direction, and the negative pressure region follows the positive pressure region. From these results, it can be observed clearly that the free field blast wave has the strong directional dependence, so that the 3-dimensional characteristics should be considered to establish the blast wave model.

B. Reflected Blast Wave

1. Oblique Shock Theory

The reflection of the free field blast wave on the surface can be broadly classified into regular reflection and Mach reflection. Figure 6 shows the schematic diagram of the reflection of gun blast wave. The incident angle α_I is the angle between the reflecting surface and the free field blast wave, and $\boldsymbol{n}$ is the surface normal vector. After firing, the free field blast, which expands in the open space at t_1, contacts the reflecting surface at t_2, and the reflecting point then moves along the reflecting surface at t_3. The reflection of the blast wave on the reflecting surface is determined by the strength of the free field blast wave and the incident angle. The regular reflection is generated in the small incident angle and it can be expressed by the analytic solution using the oblique shock theory [13,14], but Mach reflection generated beyond the incident angle can not be calculated by using the solution.

At the reflecting point on the surface, the free field and reflected blast waves can be assumed oblique plane shocks and these shocks can also be considered as fixed shocks with respect to the observer moving at the shock-wave velocity as shown in Fig. 7. Using the oblique shock theory, P_R can be calculated as follows.

Considering the incident wave as a normal shock wave, the normal components of the Mach numbers before and after the free field blast wave can be calculated as follows:

$$M_{1n} = \frac{v_S}{a_1} = \left[\frac{\gamma+1}{2\gamma}\left(\frac{P_I - P_\infty}{P_\infty}\right) + 1\right]^{1/2} \tag{13}$$

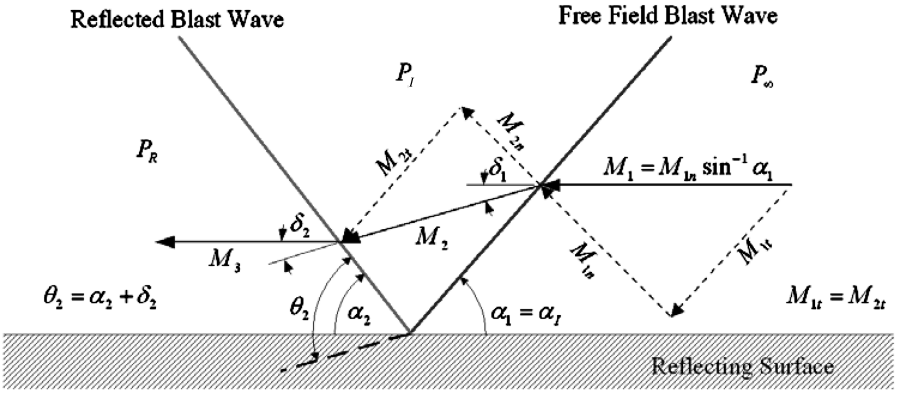

Fig. 7 Flow through fixed oblique shock waves.

$$M_{2n} = \left[\left(1 + \frac{\gamma - 1}{2} M_{1n}^2\right) \Big/ \left(\gamma M_{1n}^2 - \frac{\gamma - 1}{2}\right)\right]^{1/2} \tag{14}$$

where v_S and a_1 are the normal velocity to the free field blast wave and the sound speed in the open space, respectively. Using Eqs. (13) and (14), the Mach number behind the free field blast wave can be expressed as follows:

$$M_2 = M_{2n}\sin^{-1}(\alpha_1 - \delta_1) = \left\{\frac{[(\gamma - 1)(P_I/P_\infty) + (\gamma + 1)]}{2\gamma(P_I/P_\infty)}\right\}^{1/2} \sin^{-1}(\alpha_1 - \delta_1) \tag{15}$$

α_1 can be calculated efficiently by using the following equations described in detail in [5].

$$\alpha_1 = \cos^{-1}\frac{\boldsymbol{v}\cdot\boldsymbol{n}}{v} \tag{16}$$

$$v = (v_x^2 + v_y^2 + v_z^2)^{1/2} \tag{17}$$

where $\boldsymbol{v}$ shown in Fig. 6 is the vector directed from the boreline to the reflecting point and it is normal to the free field blast wave surface. With a little trigonometric manipulation, M_1 and δ_1 can also be obtained by the following relations:

$$M_1 = M_{1n}\sin^{-1}\alpha_1 \tag{18}$$

$$\tan\delta_1 = 2\cot\alpha_1 \frac{M_1^2\sin^2\alpha_1 - 1}{M_1^2(\gamma + \cos 2\alpha_1) + 2} \tag{19}$$

In the same manner as two equations presented above, M_2 and δ_2 can be obtained as follows:

$$M_2 = \left[\frac{\gamma + 1}{2\gamma}\left(\frac{P_R - P_I}{P_I}\right) + 1\right]^{\frac{1}{2}} \sin^{-1}\theta_2 \tag{20}$$

$$\tan\delta_2 = 2\cot\theta_2 \frac{M_2^2\sin^2\theta_2 - 1}{M_2^2(\gamma + \cos 2\theta_2) + 2} \tag{21}$$

Because of the wall condition, the deflection angles of the free field and the reflected blast waves should have the same value $\delta_1 = \delta_2$, therefore θ_2 can be calculated by Eq. (21). Finally, the reflected blast wave can be determined by using Eq. (20) as follows:

$$P_R = P_I\left[\frac{2\gamma}{\gamma + 1}(M_2^2\sin^2\theta_2 - 1) + 1\right] \tag{22}$$

The regular reflection calculated by Eq. (22) is generated in the small incident angle, so that it is necessary to determine the maximum incident angle for the regular reflection. The maximum incident angle $\alpha_{1\max}$ can be obtained by the differentiation of Eq. (19) for δ_1 as follows:

$$\frac{(-2/\sin^2\alpha_{1\max})AB + 4M_1^2(A + 2B)\cos^2\alpha_{1\max}}{A^2} = 0 \tag{23}$$

where

$$A = M_1^2(\gamma + \cos 2B) + 2 \tag{23a}$$

$$B = M_1^2\sin^2\alpha_{1\max} - 1 \tag{23b}$$

If $\alpha_1 \geq \alpha_{1\max}$, Mach reflection occurs instead of the regular reflection. It will be considered in the following section.

2. *Mach Reflection Calculation*

The flow behind Mach reflection is the combination of supersonic and subsonic flow divided by a slip line, which makes the analysis of Mach reflection extremely difficult. To obtain Mach reflection generated beyond $\alpha_{1\max}$, it is necessary to measure the reflected pressure directly or to analyze the flow field computationally. In the present study, CFD calculation using FLUENT v6.0 is performed to obtain the Mach reflection model.

Figure 8 shows the solution domain of the Mach reflection problem. The solution domain has the pressure inlet and the wall conditions. α_I can be changed by rotating the reflecting surface with a fixed center. The flow field is analyzed by the use of a 2-D unsteady explicit inviscid model. The material property of the fluid is assumed to be an ideal gas with the specific heat ratio of 1.4. The boundary condition of the interior zone is the standard atmospheric condition at sea level, and the inlet condition is determined by the static pressure

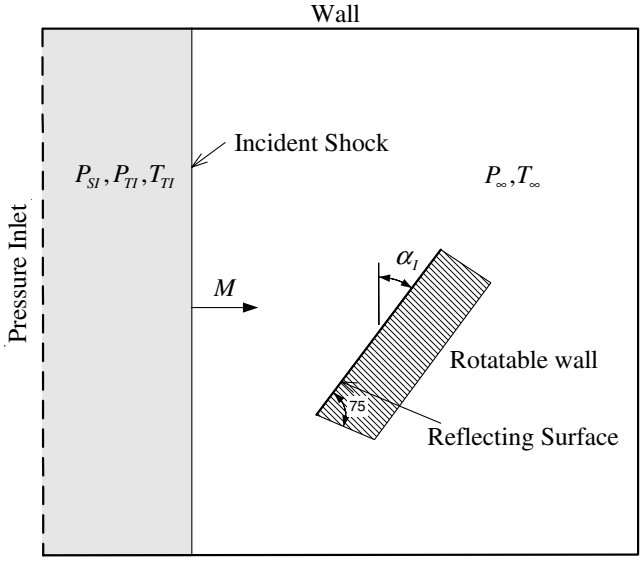

Fig. 8 Solution domain of the Mach reflection problem.

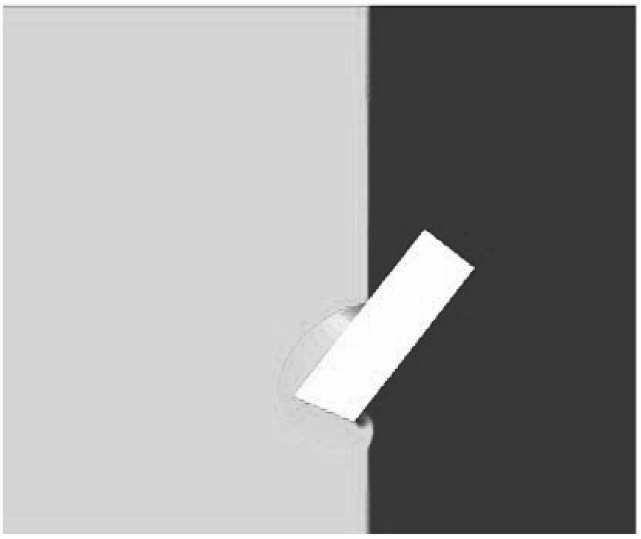

a) $\alpha_I = 38°$, regular reflection

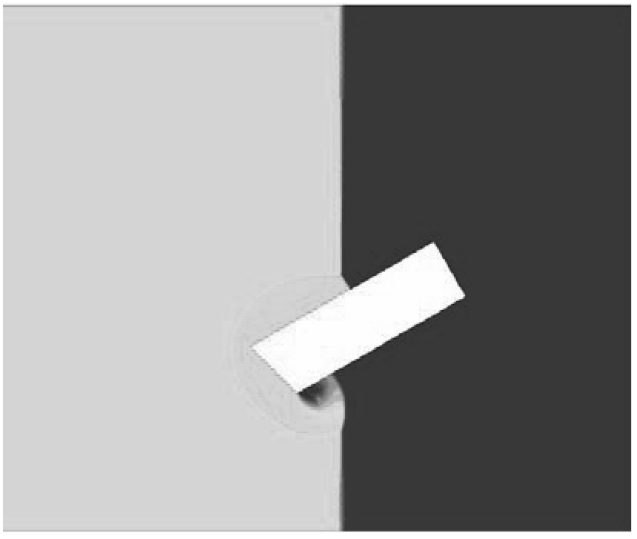

b) $\alpha_I = 60°$, Mach reflection

Fig. 9 Analysis results of the reflected shock wave for the incident overpressure of 50 psi (344.738 kPa).

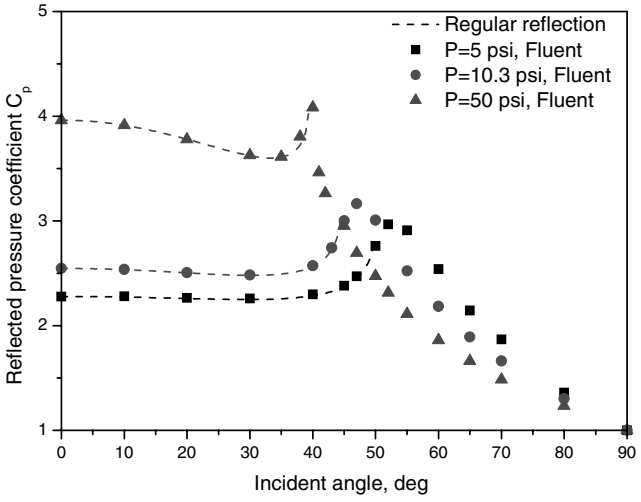

Fig. 10 Reflected pressure calculated by the regular reflection solution and CFD calculations.

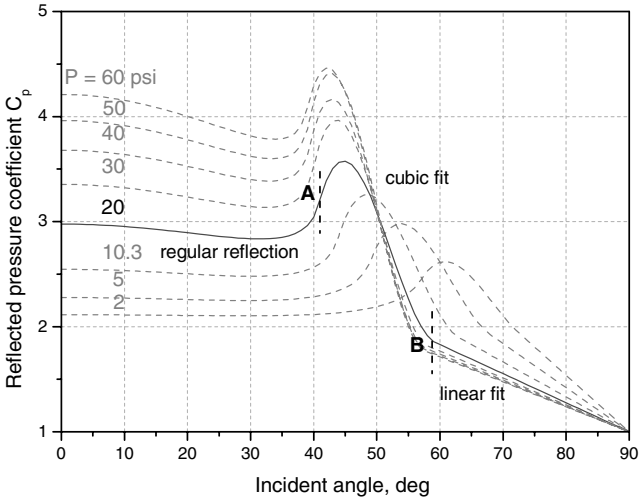

Fig. 11 Reflected pressure coefficients generated by GUNBLAST for various incident overpressures.

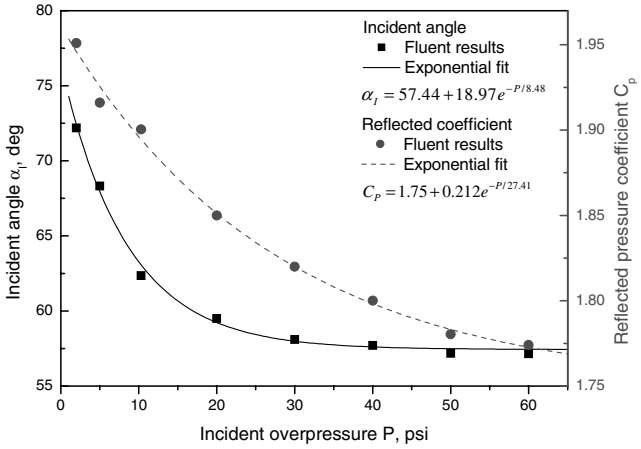

Fig. 12 Exponential fits of the incident angle and the reflected pressure coefficient at point B for various incident overpressures.

P_{SI}, the total pressure P_{TI} and the total temperature T_{TI} using an user defined function. For the solver controls, the second order upwind method is used as the discretization scheme and the Courant number is 0.3.

The CFD calculations are performed for the incident pressure range from 2 psi (13.789 kPa) to 60 psi (413.685 kPa) and the incident angle in range 0–90°. When the incident shock is standing at the center of the reflecting surface, the reflected pressure behind the reflecting point is obtained. Figure 9 shows the analysis results for the incident overpressure of 50 psi (344.738 kPa). In this case, the maximum incident angle $\alpha_{1\max}$ calculated by Eq. (23) is 39.04°. From these results, it can be observed clearly that the regular reflection appears in a relatively small incident angle and Mach reflection generates for a large incident angle. Figure 10 shows that the reflected pressures calculated by Eq. (22) in regular reflection regions are in good agreement with the results from the CFD calculations. The reflected pressure coefficient is defined as follows:

$$C_p = \frac{P_R - P_\infty}{P_I - P_\infty} \tag{24}$$

For the incident angle beyond $\alpha_{1\max}$, it is impossible to obtain an analytic solution to the reflected pressure by using the oblique shock theory. In this region the reflected pressure can be expressed by using polynomials such as a cubic fit and a linear fit as shown in Fig. 11, and the fit functions can be expressed as

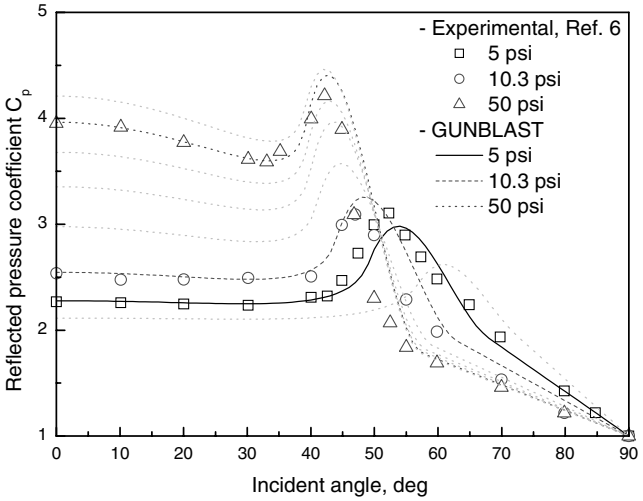

Fig. 13 Comparison the reflected pressure coefficients obtained by GUNBLAST with experiment.

$$P_y(\alpha_x) = A_0 + A_1\alpha_x + A_2\alpha_x^2 + A_3\alpha_x^3 \tag{25}$$

$$P_y(\alpha_x) = B_0 + B_1\alpha_x \tag{26}$$

For each incident overpressure, the reflected overpressure model can be obtained by joining of the regular reflection solution, the cubic and the linear fits which are divided by the point A and B. To evaluate the polynomials, it is necessary to calculate the boundary values which are the reflected pressures and the slopes at the point A and B. The boundary values at the point A can be obtained by the solution of regular reflection for each incident overpressure. However, it is impossible to determine the boundary values at the point B using an analytical solution. At this point, the reflected pressure coefficient should only be determined, because the reflected pressure coefficient always equals one at $\alpha_I = 90°$. The position of the point B varies with incident overpressure. In the present study, the exponential fit functions of the incident angle and the reflected pressure coefficient at the point B with respect to the incident overpressure are extracted from the CFD results as follows:

$$\alpha_{IB} = 57.44 + 18.97e^{-P/8.48} \tag{27}$$

$$C_{P_B} = 1.75 + 0.212e^{-P/27.41} \tag{28}$$

and they are shown in Fig. 12. Figure 13 shows that the reflected pressure coefficients obtained from this procedure are in good agreement with the experimental data in [5].

3. Blast Wave Model Verification

In the present study, the blast wave model GUNBLAST is established from the process outlined in the previous sections. Once the weapon characteristics and the launch conditions are determined, the free field blast wave at the structural surface of interest can be calculated by using Eqs. (5–7), and the incident angle can be calculated using Eq. (16) to determine whether the regular reflection or Mach reflection of the blast wave occurs for the incident pressure. If the incident angle is in the regular reflection region, Eq. (22) is used to obtain the reflected pressure. Otherwise, the point B is determined by using Eqs. (27) and (28) for the incident pressure, and Eqs. (25) or (26) are used to calculate the reflected pressure.

To verify the blast wave model, the reflected blast wave estimated by GUNBLAST is compared with the experimental data of the 30 mm chain gun whose characteristic and launch conditions are the same as those listed in Table 1. The contour map of $\bar{P}_R$ is shown in Fig. 4d. It shows that the reflected blast wave has a strong directional dependence like the free field blast wave and the peak values of the reflected pressure are much larger than those of the incident blast wave. Figure 14 shows that the peak reflected overpressure and the blast arrival time obtained by GUNBLAST agree well with the experimental data.

III. Structural Analysis for Blast Load

GUNBLAST is applied to two kinds of structural models for structural analyses using MSC/NASTRAN. First, to investigate the muzzle distance effect from the structural surface to the muzzle, the responses of a graphite epoxy composite panel exposed to the blast wave of a 12.7 mm gun are analyzed for various muzzle distances. Second, the transient response analyses of a left wing model with an external fuel tank and 12.7 mm outboard gun are carried out for the blast loads of 1 and 50 round fires with the firing rate of 17 Hz. For the latter application, the time and frequency responses at the tip of the wing are investigated.

A. Composite Panel Analysis

The structural analyses of a composite panel exposed to the blast load are performed as the first application of GUNBLAST. The panel is the graphite/epoxy composite plate with 1% structural damping whose laminate stacking sequence is $[0/\pm 45/90]_s$ and the configuration is shown in Fig. 15a. The graphite/epoxy and geometry properties are given as follows:

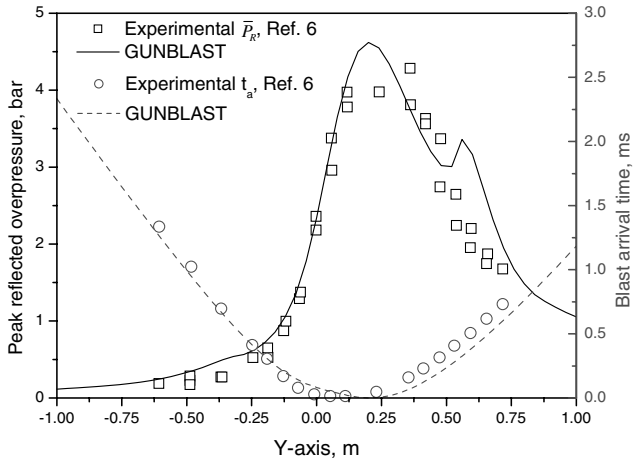

a) Parallel to the boreline

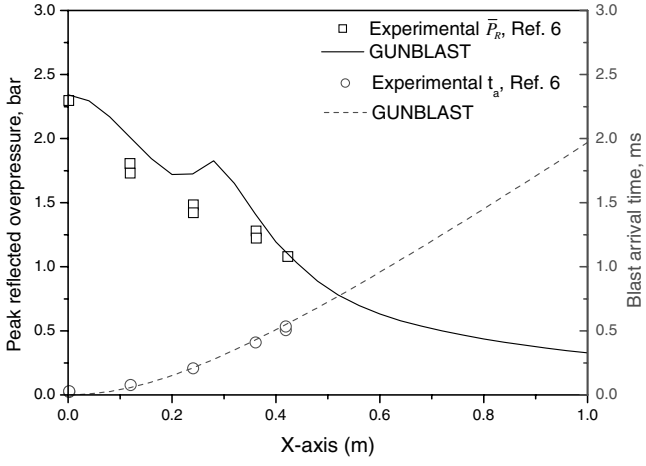

b) Perpendicular to the boreline

Fig. 14 Comparison the peak reflected overpressure and the blast arrival time by GUNBLAST with experiment for 30 mm chain gun.

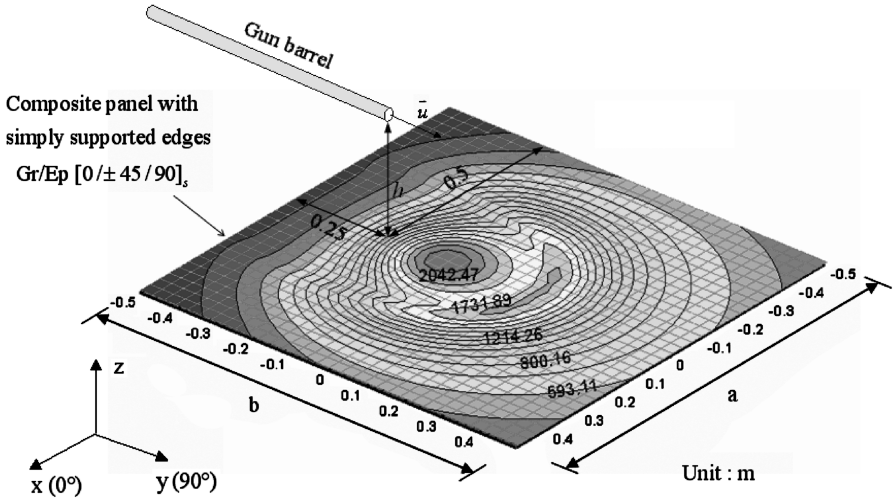

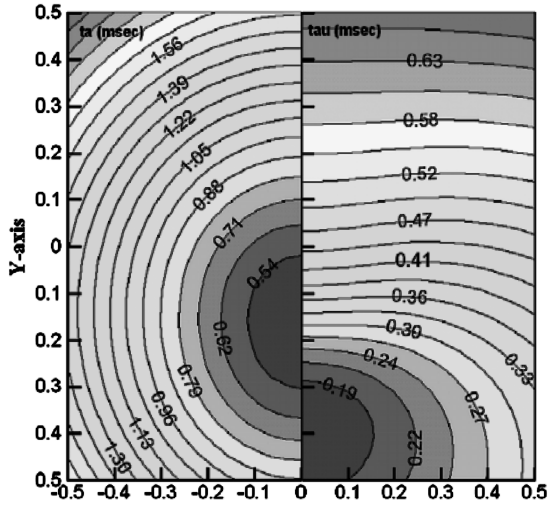

Fig. 15 Configuration of composite panel and contour maps generated by GUNBLAST for 12.7 mm gun with 0.2 m muzzle distance.

$$E_1 = 119 \text{ GPa}, \quad E_2 = 8.67 \text{ GPa}, \quad G_{12} = G_{13} = 5.18 \text{ GPa},$$
$$G_{23} = 3.29 \text{ GPa}, \quad \nu_{12} = 0.31, \quad \rho = 1570 \text{ kg/m}^3, \quad (29)$$
$$a = b = 1.0 \text{ m}, \quad h = 0.25 \text{ m}, \quad \text{and} \quad h_l = 0.125 \text{ mm}$$

where h_l means the thickness of graphite/epoxy lamina. The finite element model has $1024(32 \times 32)$ qaud-4 elements and total 6150 degrees of freedom.

Using MSC/NASTRAN, the direct transient responses of the plate to the gun blast wave of a 12.7 mm gun are analyzed for several muzzle distances in the range of 0.1–10 m. The geometric nonlinearity is not included and the time step size is 0.1 msec. The weapon characteristics and the launch conditions of the gun are listed in Table 1. Figure 15 shows the parameter contour maps generated by GUNBLAST for the muzzle distance of 0.2 m.

In this application, the normalized rms deviations of the parameters on the panel are calculated for each muzzle distance, and the deviation is defined as follows:

$$\sigma[\hat{\phi}] = \frac{\sqrt{E[(\hat{\phi} - \phi)^2]}}{\hat{\phi}} \quad (30)$$

with

$$\hat{\phi} = E[\phi] \quad (31)$$

where ϕ and E are the parameter value at each grid point and the average of the parameters, respectively. Figure 16 shows that the normalized rms deviations decrease exponentially with respect to the muzzle distance. Figure 17 shows the comparison of the time responses at the center of the panel for the blast load generated by

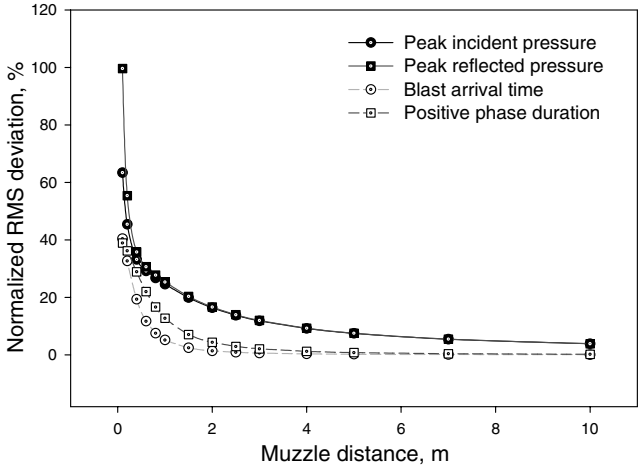

Fig. 16 Normalized rms deviation of gun blast load on the panel vs muzzle distance.

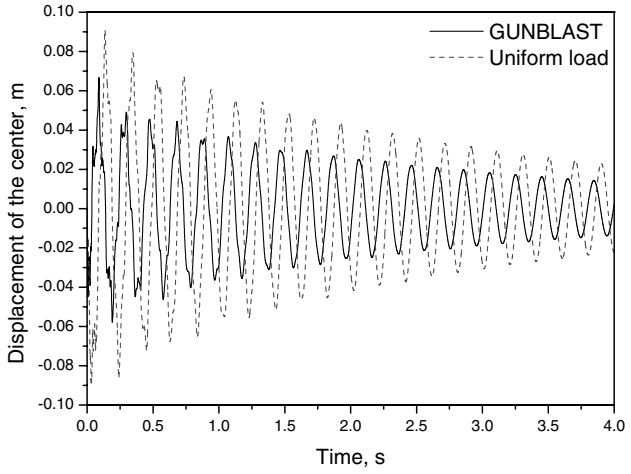

a) Muzzle distance of 0.2 m

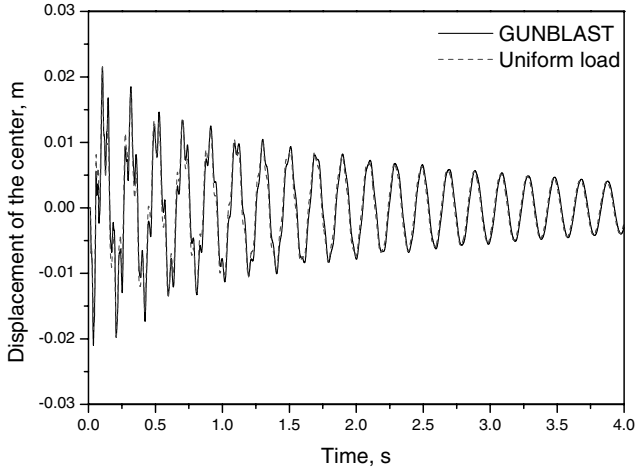

b) Muzzle distance of 5 m

Fig. 17 Comparisons of the displacements at the center of the panel for GUNBLAST and uniform load.

GUNBLAST and the uniform load composed of the mean values of the parameters. It shows clearly the difference between the two displacements at the muzzle distance of 0.2 m, as well as the concordance at the muzzle distance of 5.0 m. From the results, it can be observed that the assumption of the uniform blast wave for the surface can be applicable beyond the muzzle distance of about 3 m, but the 3-dimensional characteristics of the gun blast wave should be considered within the distance.

B. Aircraft Wing Analysis

As the second application of GUNBLAST, the structural response of an aircraft left wing shown in Fig. 18 is analyzed for the gun blast load. The chord length of the wing is 1.9 m and the span length is 4.8 m. The wing is equipped with one external fuel tank and the 12.7 mm outboard gun which are located at 1.86 and 2.76 m from the root, respectively. The finite element model has 808 nodes and 1999 elements which consist of bar-2, quad-4, tria-3 and point elements. The clamped boundary condition is applied to the root and the model has 2% structural damping. Figure 19 shows the parameter contour maps of the lower surface for the gun blast load generated by GUNBLAST. The direct transient response analyses using MSC/NASTRAN are performed for 1 and 50 round repeated fires with the firing rate of 17 Hz. The geometric nonlinearity is not included and the time step size is 0.1 msec.

Figure 20 shows the vertical displacements at the wing tip for the blast loads. From the results, we can find that the response resulting from the gun blast load is not negligible, though the clamped wing

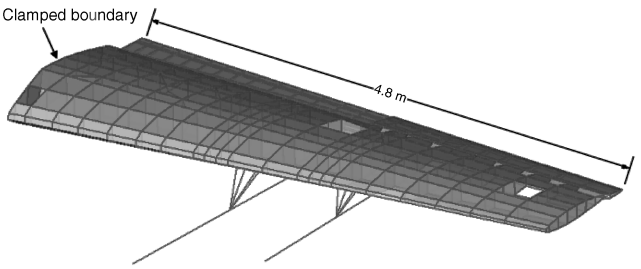

Fig. 18 Structural model of aircraft left wing with external fuel tank and 12.7 mm outboard gun.

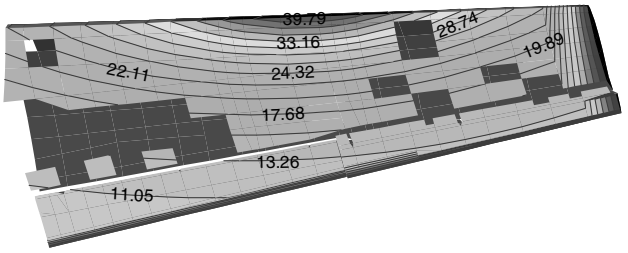

a) $\bar{P}_I$, mbar

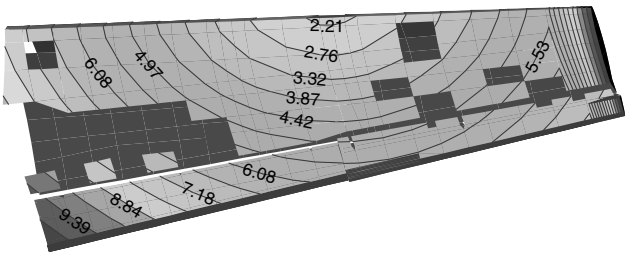

b) t_a, ms

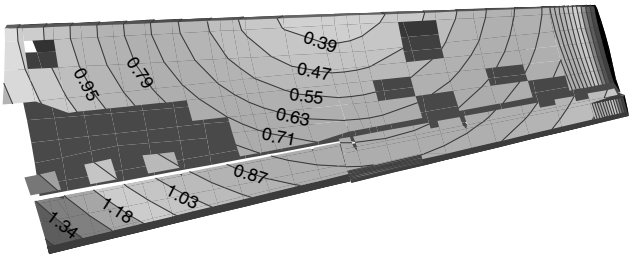

c) τ, ms

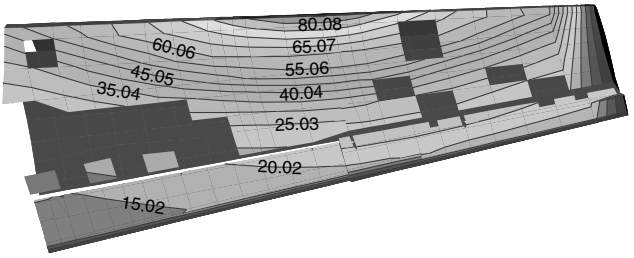

d) $\bar{P}_R$, mbar

Fig. 19 Left wing contour maps generated by GUNBLAST for 12.7 mm outboard gun.

model is considered in this study. Figure 21 shows the acceleration power spectral density at the wing tip in vertical direction. It is clear that the vibration due to the gun blast wave is a combination of broadband random vibration and harmonic peaks at the firing rate frequency. This vibration may cause structural fatigue failure or high

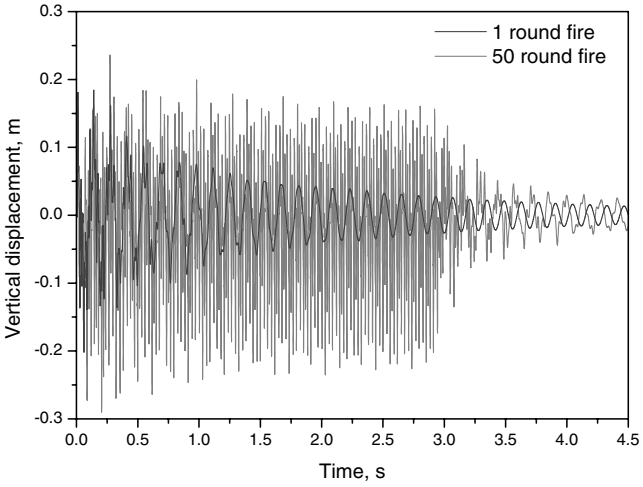

Fig. 20 Vertical displacements at wing tip for 1 and 50 round fires.

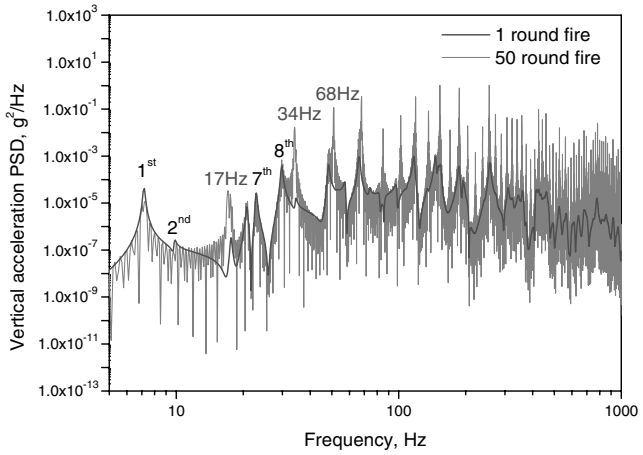

Fig. 21 Vertical acceleration power spectral density for 1 and 50 round fires.

frequency damage to the structure and equipment mounted in the aircraft. Therefore, the vibration levels resulting from the gun blast load should be predicted exactly for the structural and functional safety.

IV. Conclusion

The gun blast wave model GUNBLAST which can be applied to various guns, is established. The fundamental shape of the blast wave is represented by the Friedlander waveform. The scaling approach is used for modeling of the free field blast wave. To calculate the reflection of the free field blast wave on the structural surface, the regular reflection and Mach reflection are considered. The analytic solution of the regular reflection is obtained by the use of the oblique shock theory, and Mach reflection is calculated numerically by using FLUENT. From the result, the polynomial functions for the reflection of the blast wave are suggested. Finally, GUNBLAST is verified with experimental data and it is then applied to two kinds of structural models. The structural response of the composite panel exposed to the gun blast load is analyzed to investigate the muzzle distance effect, and the transient response analysis of the left wing is carried out to clarify the vibration characteristics resulting from the repeated blast load. From the results, it can be shown that the established blast wave model can be applicable to not only the prediction and reduction of the vibration resulting from the gun blast wave, but also a weight-optimized, blast resistant structure design which are fabricated and attached to an aircraft.

References

[1] Erdos, J. I., and Del Guidice, P. D., "Calculation of Muzzle Blast Flowfields," *AIAA Journal*, Vol. 13, No. 8, 1975, pp. 1048–1055.

[2] Schmidt, E. M., and Shear, D. D., "Optical Measurements of Muzzle Blast," *AIAA Journal*, Vol. 13, No. 8, 1975, pp. 1086–1091.

[3] Moretti, G., "A Numerical Analysis of Muzzle Blast Precursor Flow," *Computers and Fluids*, Vol. 10, No. 1, 1982, pp. 51–86.

[4] Fansler, K. S., "Dependence of Free-Field Impulse on the Decay Time of Energy Efflux for a Jet Flow," *The Shock and Vibration Bulletin*, Naval Research Laboratory, Washington, DC, Bulletin 56, 1986, pp. 203–212.

[5] Heaps, C. W., Fansler, K. S., and Schmidt, E. M., "Computer Implementation of a Muzzle Blast Prediction Technique," *The Shock and Vibration Bulletin*, Naval Research Laboratory, Washington, DC, Bulletin 56, 1986, pp. 213–229.

[6] Gupta, A. D., Gregory, F. H., Bitting, R. L., and Bhattacharya, S., "Dynamic Analysis of an Explosively Loaded Hinged Rectangular Plate," *Computers and Structures*, Vol. 26, No. 1–2, 1987, pp. 339–344.

[7] Louca, L. A., Pan, Y. G., and Harding, J. E., "Response of Stiffened and Unstiffened Plates Subjected to Blast Loading," *Engineering Structures*, Vol. 20, No. 12, 1998, pp. 1079–1086.

[8] Na, S. S., and Librescu, L., "Dynamic Response of Elastically Tailored Adaptive Cantilevers of Nonuniform Cross Section Exposed to Blast Pressure Pulses," *International Journal of Impact Engineering*, Vol. 25, Issue 9, 2001, pp. 847–867.

[9] Librescu, L., Oh, S-Y., and Hohe, J., "Linear and Non-Linear Dynamic Response of Sandwich Panels to Blast Loading," *Composites B*, Vol. 35, No. 6–8, 2004, pp. 673–683.

[10] Librescu, L., Na, S. S., Marzocca, P., Chung, C. H., and Kwak, M K., "Active Aeroelastic Control of 2-D Wing-Flap Systems Operating in an Incompressible Flowfield and Impacted by a Blast Pulse," *Journal of Sound and Vibration*, Vol. 283, No. 3-5, 2005, pp. 685–706.

[11] Turkmen, H. S., "Structural Response of Laminated Composite Shells Subjected to Blast Loading: Comparison of Experimental and Theoretical Methods," *Journal of Sound and Vibration*, Vol. 249, No. 4, 2002, pp. 663–678.

[12] Baker, W. E., *Explosions in Air*, University of Texas Press, Austin, 1973.

[13] Liepmann, H. W., and Roshko, A., *Elements of Gasdynamics*, John Wiley & Sons, New York, 1957.

[14] John, J. E. A., *Gas Dynamics*, 2nd ed., Allyn and Bacon, Boston, 1984.

[15] Settles, G. S., *Schlieren and Shadowgraph Techniques*, Springer–Verlag, New York, 2001.